Applied Catalysis B: Environmental 90 (2009) 321–329

Contents lists available at ScienceDirect

Applied Catalysis B: Environmental

journal homepage: www.elsevier.com/locate/apcatb

Synergistic effect of TiO_2 and iron oxide supported on fluorocarbon films Part 2: Long-term stability and influence of reaction parameters on photoactivated degradation of pollutants

F. Mazille [a], A. Lopez [b], C. Pulgarin [a,*]

[a] Institute of Chemical Sciences and Engineering, SB, GGEC, Ecole Polytechnique Fédérale de Lausanne, 1015 Lausanne, Switzerland
[b] Istituto di Ricerca Sulle Acque C.N.R., Via F. De Blasio 5, 70123 Bari, Italy

ARTICLE INFO

Article history:
Received 18 February 2009
Received in revised form 29 April 2009
Accepted 1 May 2009
Available online 9 May 2009

Keywords:
Heterogeneous photo-Fenton
TiO_2 photocatalysis
pH and temperature effect
Solar detoxification

ABSTRACT

The degradation of hydroquinone (HQ) and nalidixic acid (NA) mediated by TiO_2 and iron oxide immobilized on functionalized polyvinyl fluoride films (PVF^f–TiO_2–Fe oxide) in the presence of H_2O_2 under simulated solar light has been examined. The results show that the contribution of homogeneous photo-Fenton oxidation to the initial mineralization process was low. The degradation rates were not dependant of initial pH. Heterogeneous photocatalytic activity of PVF^f–TiO_2–Fe oxide was enhanced by increasing temperature, NaCl addition and by long-term utilization.

The PVF^f–TiO_2–Fe oxide surface was characterized by scanning electron microscopy (SEM) and X-ray photoelectron spectroscopy (XPS) at different states of utilization. Correlations between the catalyst surface composition and degradation kinetics are discussed. Long-term stability evaluated by repetitive pollutant degradations was outstanding. The presence of TiO_2 seems to (i) limit contact between polymer film and highly reactive radicals in the solution and (ii) act as a charge trap. Moreover, during the photocatalysis mediated by PVF^f–TiO_2–Fe oxide, some leaching of supported iron increased the amount of the top TiO_2 layer exposed to the light increasing the synergistic effects between the two oxides leading to enhanced pollutant degradation.

1. Introduction

The aimed characteristics for supported TiO_2–Fe oxide as heterogeneous photocatalysts are: (i) low leaching out of photo-active species from support surface during operation; (ii) adequate degradation rates at neutral pH and under solar illumination; (iii) resistance of support to oxidation by radicals in solution; (iv) catalyst showing long-term stability and (v) catalyst manufacture should be sustainable from the environmental and economical point of view.

Some recent studies described TiO_2–Fe oxide coatings on different supports [1–2] including polymer films [3]. However the effect of pH, temperature on rates has not been reported. In the case of supported heterogeneous photo-Fenton systems [4–11], degradation rates are strongly pH-dependant with highest performance at pH 3 and lower as we move to neutral initial pH. In these systems, the degradation rates increase as the temperature increases [6]. The effect of NaCl content on rates is also an important issue because of the utilization of sea water in some industrial processes.

The dissolution of iron ions is a common phenomenon during heterogeneous photo-Fenton oxidation. In the presence of ligands (aliphatic acids, humic acids ...) and light, particularly under acidic conditions, iron is released by photo-reductive dissolution increasing the contribution of homogeneous photo-Fenton reaction [12–14].

The sequential preparation of PVF^f–TiO_2–Fe oxide by TiO_2 photocatalytic surface functionalization-deposition (TiO_2 PSFD) treatment of PVF followed by forced hydrolysis of a $FeCl_3$ solution was described in detail in a previous study [3]. PVF^f–TiO_2–Fe oxide can be described as a highly efficient photocatalyst due to synergistic effects of TiO_2 and iron oxide deposited on functionalized PVF film.

In this work, hydroquinone (HQ) has been selected as a model substance whereas nalidixic acid was used because it is an antibiotic present in a real saline pharmaceutical wastewater. The objectives of this study are: (i) to examine the performance of PVF^f–TiO_2–Fe oxide in the degradation of HQ and NA under different reaction conditions (pH, temperature, NaCl content), (ii) correlate the photo-activity enhancement to the surfaces modifications and (iii) to test the long-term stability of the catalyst.

* Corresponding author. Tel.: +41 21 693 4720; fax: +41 21 693 6161.
E-mail address: cesar.pulgarin@epfl.ch (C. Pulgarin).

0926-3373/$ – see front matter © 2009 Elsevier B.V. All rights reserved.
doi:10.1016/j.apcatb.2009.05.004

2. Experimental

2.1. Chemicals

Hydroquinone ($C_6H_6O_2$), nalidixic acid ($C_{12}H_{12}N_2O_3$), NaOH, NaCl, HNO_3, $FeCl_3$, $FeSO_4{\cdot}7H_2O$, ferrozine, hydroxylamine hydrochloride, acetate buffer (pH 4.65) were Fluka p.a. reagents (Buchs, Switzerland) and used as received. Hydrogen peroxide (35 wt.%) was supplied by Merck AG (Darmstadt, Germany) and TiO_2 P25 (anatase to rutile weight ratio between 70:30 and 80:20) by Degussa. The Tedlar® is a DuPont film (thickness 72 μm) and consists of (–CH_2–CHF–) structural groups. The film is tough, flexible and fatigue-resistant up to 180 °C (flowing point).

2.2. Photocatalyst preparation

The detailed preparation procedure was described in a previous paper, part 1 of this work [3]. In the present study, a TiO_2 PSFD treatment of 2 h was applied to PVF film using aqueous TiO_2 suspensions (1 g/L) at natural initial pH (≈5) and under simulated sunlight irradiation leading to PVF^f–TiO_2.

For iron oxide coating, PVF and PVF^f–TiO_2 were immersed in an aqueous solution of $FeCl_3$ (5 g/L) and heated at 80 °C under stirring for 1 h. Then the resulting materials were dried in an oven at 100 °C during 1 h.

2.3. Photoreactor and irradiation procedure

The photoreactor setup and the lamp characteristics were described in a previous paper [3]. All the homogeneous (Fe^{2+} 0.3 or 2 mg/L) and heterogeneous (PVF–Fe oxide, PVF^f–TiO_2–Fe oxide 75 cm^2) photo-Fenton degradation experiments were performed with fresh synthetic HQ and NA solutions (0.18 mM) adding 1.6 and 3.2 mM H_2O_2, respectively. The natural pHs for HQ and NA were 5.7 and 6.5 and were not adjusted before the treatment. The irradiation experiments were started at room temperature (20 °C) and progressively the temperature increased up to approximately 30 °C. For the assessment of temperature dependence, the reactors were heated to the desired value with a hot plate (RTC basic IKA) equipped with a thermostat (ETC 04 fuzzy from IKA). For the study of the influence of salt content, NaCl solution (5 g/L) was used.

2.4. Analysis of the irradiated solutions

The quantitative determination of organic compounds was carried out by HPLC chromatography using a LC system HPLC–UV: Shimatzu LC-2010A equipped with a UV detector. Samples were injected via an auto-sampler. Samples of the treated HQ solution were eluted at a flow rate of 1 mL min^{-1} through a column (nucleosil C18 Marcherey Nagel) and using as mobile phase HPLC grade acetonitrile–acetic acid solution (10%) in a 40–60%. Samples of the treated NA solution were eluted at a flow rate of 1 mL min^{-1} through a column (nucleosil C8 HPLC) and using as mobile phase HPLC grade acetonitrile–formic acid solution (25 mM) in a 50–50%. Total organic carbon (TOC) was monitored via an instrument (Shimadzu 500) equipped with an automatic sample injector (ASI). The peroxide concentrations were assessed by Merkoquant® paper at levels between 0.5 and 25 mg/L. The analyses were performed as fast as possible after sampling in order to minimize the effect of dark Fenton reaction.

The total iron concentration in the irradiated solutions was measured by complexing with Ferrozine® (Aldrich 16.060-1) in the presence of hydroxylamine hydrochloride and of acetate buffer (pH 4.65) [15]. The pH values were measured with a pH electrode SenTixH WPW connected to a pH 330i WTW device.

2.5. Photocatalyst characterization

2.5.1. X-ray photoelectron spectroscopy (XPS)

X-ray photoelectron spectroscopy data were collected by Axis Ultra system (Kratos analytical, Manchester, UK) under ultra-high vacuum condition ($<10^{-8}$ Torr), using a monochromatic Al K_α X-ray source (1486.6 eV) at the laboratory of Chemical Metallurgy at EPFL. The source power was maintained at 150 W (10 mA, 15 kV). The emitted photoelectrons were sampled from a square area of 750 μm × 350 μm. The gold (Au $4f_{7/2}$) and copper (Cu $2p_{3/2}$) lines at 84.0 and 932.6 eV, respectively, were used for calibration, and the adventitious carbon 1s peak at 284.6 eV was used as an internal standard to compensate for charging effects.

2.5.2. Secondary electron microscopy (SEM) analysis

The surface morphology of the supports and the catalysts was investigated with a scanning electron microscope (Phillips XL30 SFEG) equipped with X-ray detector.

3. Results and discussion

3.1. Photocatalytic activity toward hydroquinone and nalidixic acid degradation

Fig. 1 presents the evolution of HQ and TOC concentrations within 240 min under different conditions. Trace a shows that HQ mineralization induced by the homogeneous photo-Fenton oxidation (Fe^{2+}(0.3 mg/L)/H_2O_2/light) reached around 60%. For the system PVF–Fe oxide/H_2O_2/light (trace b), the TOC concentration increased during the first 30 min, due to PVF degradation by generated radicals, and thereafter rapidly decreased to reach 80% of mineralization after 240 min. For the system PVF^f–TiO_2–Fe oxide/H_2O_2/light (trace c), the TOC removal was faster, reaching a mineralization of 95% and the half-life time was about 20 min for HQ (trace d) under these conditions.

A comparison between traces b and c in Fig. 1 shows the beneficial effect induced by the TiO_2 PSFD treatment.

These results show that the presence of a TiO_2 layer between functionalized polymer surface and iron oxide layer prevents the degradation and dissolution of PVF (induced by photo-Fenton reactions in the case of PVF–Fe oxide) and accelerates degradation process.

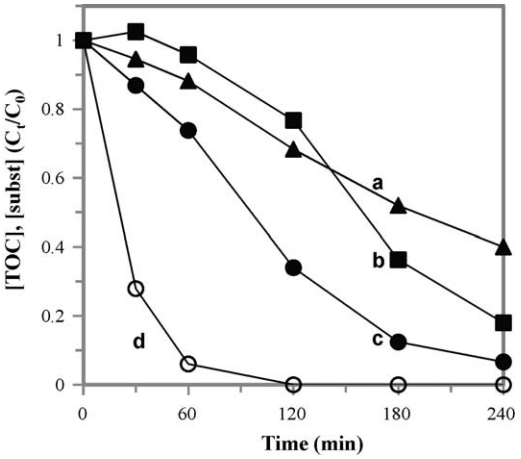

Fig. 1. Degradation of 0.18 mM of HQ, initial pH 5.7, 30 °C, 1.6 mM H_2O_2, 75 cm^2 of heterogeneous photocatalyst under solar simulation. (a) TOC removal by 0.3 mg/L Fe^{2+}/H_2O_2/light; (b) TOC removal by PVF–Fe oxide/H_2O_2/light; (c) TOC removal by PVF^f–TiO_2–Fe oxide/H_2O_2/light; (d) HQ degradation by PVF^f–TiO_2–Fe oxide/H_2O_2/light. The traces represent an average over three runs.

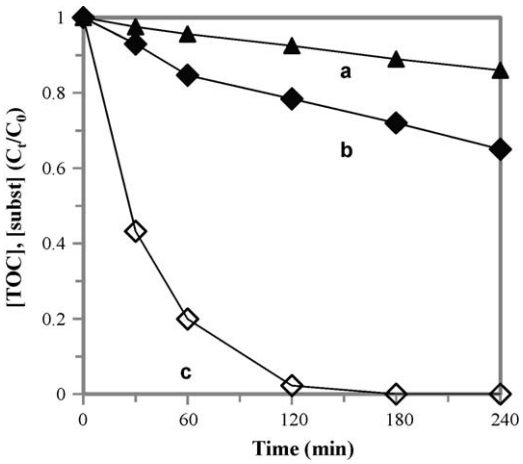

Fig. 2. Degradation of 0.18 mM of NA, initial pH 6.5, 30 °C, 3.2 mM H_2O_2, 75 cm^2 of PVF^f–TiO_2–Fe oxide under solar simulation. (a) TOC removal by 0.3 mg/L Fe^{2+}/H_2O_2/light; (b) TOC removal by PVF^f–TiO_2–Fe oxide/H_2O_2/light; (c) NA degradation by PVF^f–TiO_2–Fe oxide/H_2O_2/light. The traces represent average over three runs.

Fig. 2 presents the evolution of normalized NA and TOC concentrations within 240 min under different conditions. During homogeneous photo-Fenton (Fe^{2+}(0.3 mg/L)/H_2O_2/light) oxidation (trace a), mineralization of NA was very slow (15%). For the system PVF^f–TiO_2–Fe oxide/H_2O_2/light (trace b) the mineralization was higher (35%) and NA degradation (trace c) was fast with a half-time around 25 min.

3.2. Iron leaching and homogeneous photocatalytic contribution

Fig. 3 shows the evolution of dissolved iron concentration ($[Fe]_d$) during the photocatalytic processes measured by the ferrozine method. For HQ degradation by the system PVF–Fe oxide/H_2O_2/light, (curve a), $[Fe]_d$ increased during the first 120 min of treatment up to 0.6 mg/L and stabilized during the following 120 min. For HQ degradation by the system PVF^f–TiO_2–Fe oxide/H_2O_2/light (curve b), $[Fe]_d$ reached a maximum at 120 min with about 0.6 mg/L and decreased to 0.1 mg/L during the following 120 min. This phenomenon was also observed by other authors with different heterogeneous photocatalysts containing iron [16,17]. In the case of NA photocatalytic degradation by the system PVF^f–TiO_2–Fe oxide/H_2O_2/light, $[Fe]_d$ increased during the first 120 min of treatment up to 0.3 mg/L (trace c).

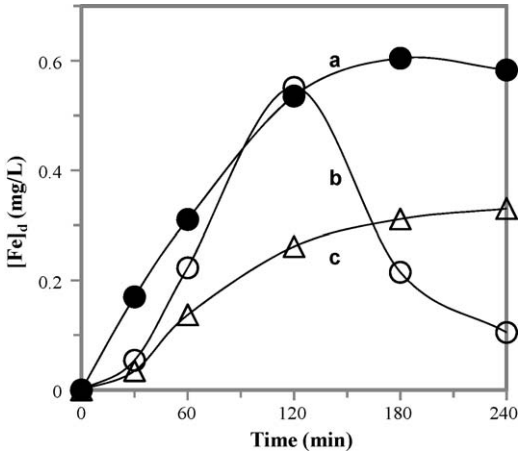

Fig. 3. Evolution of dissolved iron concentration during degradation of 0.18 mM of pollutant, initial pH 5.7, 30 °C, 75 cm^2 of heterogeneous photocatalyst under solar simulation. (a) HQ, PVF–Fe oxide/H_2O_2 (1.6 mM)/light; (b) HQ, PVF^f–TiO_2–Fe oxide/H_2O_2 (1.6 mM)/light; (c) NA, PVF^f–TiO_2–Fe oxide/H_2O_2 (3.2 mM)/light. The traces represent average dissolved iron over three runs.

When evaluating a catalyst based on iron oxide in the presence of H_2O_2, it is essential to know the amount of leached soluble iron species into the aqueous solution during photocatalytic operation and to estimate the relative contribution of homogeneous photo-Fenton reaction to the overall degradation process.

For this purpose, average dissolved iron concentration ($[Fe]_d^{av}$, Eq. (1)), TOC removal ($\Delta[TOC]_t = [TOC]_0 - [TOC]_t$), ratio r (Eq. (2)) and homogeneous percentage h_t (Eq. 3) were calculated for different photocatalytic processes and times.

$$[Fe]_d^{av} = \frac{\int_0^t [Fe]_d dt}{t} \quad (1)$$

$$r = \frac{\Delta[TOC]_t}{[Fe]_d^{av}} \quad (2)$$

$$h_t = \frac{100 \times r_{Fe^{2+}}}{r_{PVF^f-TiO_2-Fe}} \quad (3)$$

Table 1 shows that for the system PVF–Fe–oxide/H_2O_2/light, h_{60}, h_{120} and h_{240} are 100%. Thus HQ mineralization by this system seems only due to homogeneous photo-Fenton oxidation. For HQ mineralization by the system PVF^f–TiO_2–Fe oxide/H_2O_2/light, h_{60}, h_{120} and h_{240} were about 20%, 39%, and 53%, respectively, whereas for NA, h_{60}, h_{120} and h_{240} were about 8%, 16%, and 29%, respectively. This result suggests that the homogeneous contribution is significant particularly for HQ when the whole time is taken into account. However heterogeneous process is responsible for a major part of the mineralization process at the beginning of the treatment and for NA.

3.3. Initial activation of PVF^f–TiO_2–Fe oxide photocatalyst

Fig. 4(i) shows the TOC removal during HQ degradation by the system PVF^f–TiO_2–Fe oxide/H_2O_2/light during the first two catalytic operations. During the first run (trace a), the TOC increased (until 30 min) due to degradation of the PVF inducing dissolution of organic compounds and finishing polymer surface functionalization. After 240 min of treatment, the TOC removal reached 85%. In the second run (trace b), the TOC decreased from the beginning of the treatment reaching a removal of 95% after 240 min.

Fig. 4(ii) shows the evolution of dissolved iron characteristic for the two first HQ degradations as a function of time. For the first run, $[Fe]_d$ reaches a maximum of 0.6 mg/L after 120 min treatment and then stabilized around 0.5 mg/L whereas for the second run, $[Fe]_d$ reaches a maximum of 0.6 mg/L after 120 min treatment and then decreases rapidly until a value of 0.1 mg/L after 240 min. These differences in the extent of iron leaching can be attributed to the washing of loosely bounded iron during the first run. Additionally the functionalization of polymer surface (oxygen groups formation) leads to the formation of vacant sites where iron species are

Table 1
Contribution of homogeneous photo-Fenton oxidation (percentage) relative to different processes and times (values calculated from Figs. 1–3).

Photo-Fenton processes	h_{60}	h_{120}	h_{240}
(0.3 mg/L Fe^{2+}) HQ	100	100	100
PVF–Fe oxide HQ	100	100	100
PVF^f–TiO_2–Fe oxide HQ	20	39	53
(0.3 mg/L Fe^{2+}) NA	100	100	100
PVF^f–TiO_2–Fe oxide NA	5	16	29

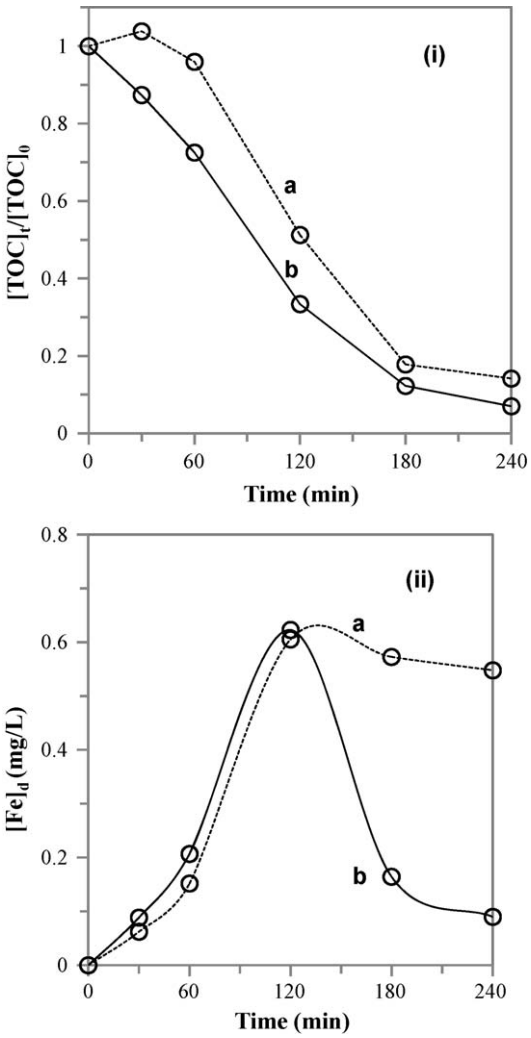

Fig. 4. Evolution of (i) normalized TOC concentration and (ii) dissolved iron concentration during the two first photocatalytic mineralization of HQ: (a) first; (b) second run (experimental conditions: 0.18 mM HQ, initial pH 5.7, 30 °C, 1.6 mM H_2O_2, 75 cm^2 of heterogeneous photocatalyst under solar simulation).

likely to form complexes at the end of the second run. Fig. 4(ii) (trace b) shows a singular pulse shape illustrating the re-adsorption of dissolved iron is much faster compare to other heterogeneous catalysts containing iron species [16,17].

3.4. Correlations between surface modifications and activation processes

3.4.1. X-ray photoelectron spectroscopy (XPS) analysis of PVF^f–TiO_2–Fe oxide

The XPS spectroscopy allows determining surface composition of thin outermost surface layer (few nm). In all the spectra there was an energy shift to lower binding energies (BE) of about 3 eV, which occurred due to the low conductivity of the samples. In the present study, the corrected BEs are given.

The differences in the chemical composition of PVF^f–TiO_2–Fe oxide surface before and after three photocatalytic runs were

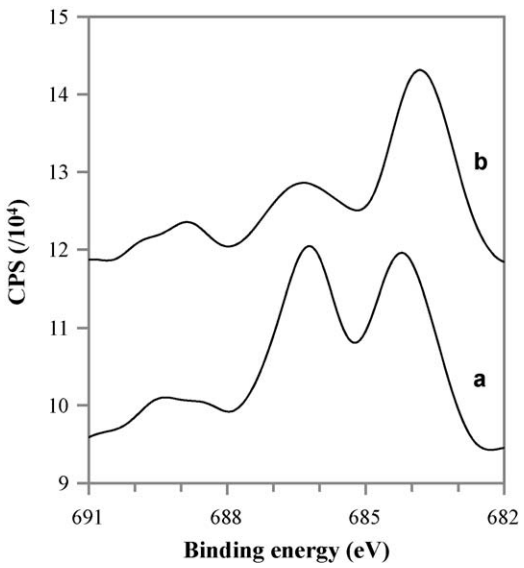

Fig. 5. F (1s) photoelectron spectra of (a) PVF^f–TiO_2–Fe oxide as prepared and (b) PVF^f–TiO_2–Fe oxide after three runs.

investigated by XPS. Fe (2p) photoelectron spectrum was not significantly changed due to usage (results not shown). Table 2 shows the variation of surface atomic composition induced by PVF^f–TiO_2–Fe oxide utilization. Before use, a relatively high amount of iron (23.8%) was found. The presence of important surface atomic concentration of chloride (6.4%) suggests that the nature of oxide was probably akaganeite (β-$FeOOH{\cdot}Cl_n$). XPS results show as well that oxygen, fluorine, chlorine and iron relative surface concentrations decrease after the degradation runs but the concentration of carbon increases. The drastic Fe/C ratio fall from 1.05 to 0.47 on PVF^f–TiO_2–Fe oxide composite after utilization can be allocated to erosion of the surface induced by the washing or photo-leaching of iron species and to physical or chemical adsorption of organic compounds. The depletion of fluorine concentration can be explained by the degradation of the polymer surface during irradiation whereas the depletion of chlorine concentration can be allocated to anion exchange properties of akaganeite. Akaganeite is tunnel structured containing interstitial Cl^- that can be substituted by other small anions like F^-, OH^- [18]. In Fig. 5, the photoelectron spectrum of F (1s) core level of PVF^f–TiO_2–Fe oxide is represented. Before utilization (trace a), the F (1s) peak is triple with two predominant components at BEs of 684.2 and 686.3 eV, corresponding to fluorine incorporated into iron oxide (FeOF) due to the anion exchange properties of akaganeite, and to polymeric C–F bond, respectively. The small third F (1s) peak centered at a BE = 689 eV corresponds to F^- absorbed at iron oxide surface. After third run (trace b), the main difference is that the central peak corresponding to polymeric fluorine (C–F bond) decreased, pointing out that during HQ degradations mediated by PVF^f–TiO_2–Fe oxide, the polymer surface continues to undergo modifications. Fig. 5 suggests as well that fluorides from the polymer are incorporated into the tunnel sites and surface sites of akaganeite, and exchanges of Cl^- by OH^- may occur as well. Moreover leaching of iron during utilization uncovers a part of the TiO_2 that was previously totally

Table 2
Composition of PVF^f–TiO_2–Fe oxide surface (atomic percent) as prepared and after three runs.

Samples	C	O	F	Cl	Ti	Fe	Fe/C	Fe/Ti	Fe/Cl
PVF^f–TiO_2–Fe oxide	22.7	46.0	2.0	6.4	0	23.8	1.05	–	3.72
PVF^f–TiO_2–Fe oxide after use	35.1	45.1	1.5	1.7	0.3	16.8	0.47	56	9.88

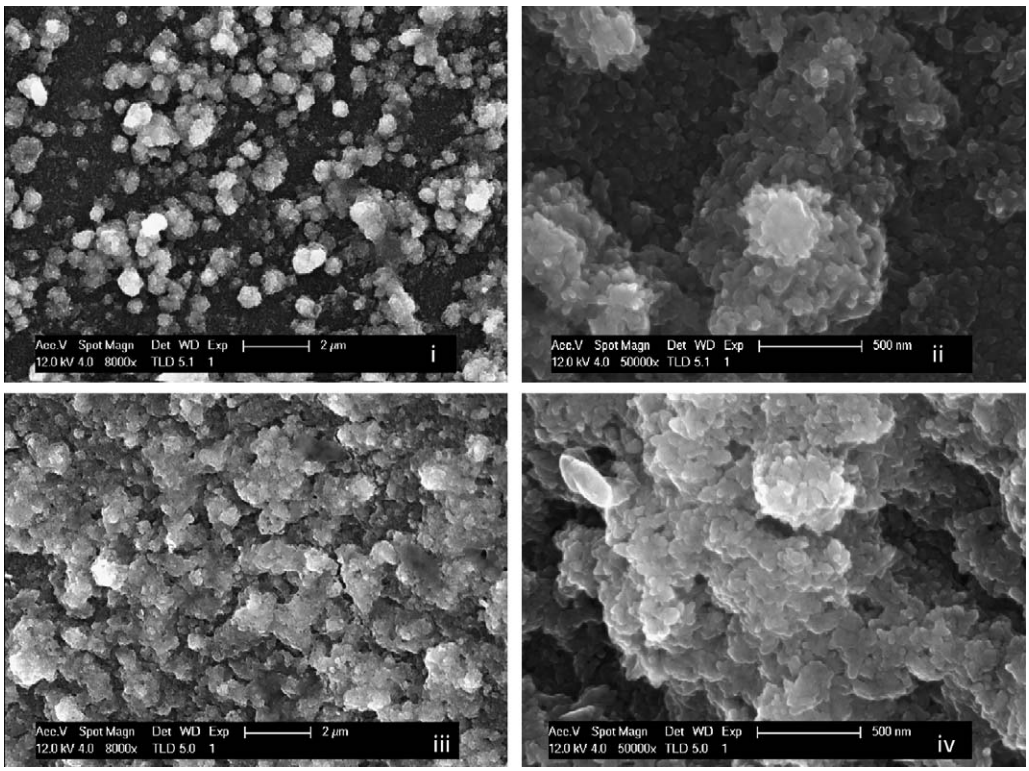

Fig. 6. Scanning electron microscopic images of PVF^f–TiO_2–Fe oxide (i)–(ii) before and (iii)–(iv) after three runs.

covered by iron oxide. Table 2 shows that after three runs, 0.3% of atomic surface composition is constituted by titanium. The presence of TiO_2 at material surface plays a central role in the observed activation and synergistic processes.

3.4.2. Secondary electron microscopy (SEM)

Fig. 6 shows the catalyst surface morphology before and after utilization. In Fig. 6(i) the PVF^f–TiO_2–Fe oxide surface with iron oxide aggregates of about 1 μm is shown. These aggregates are composed of nanoparticles of approximately 50 nm, which seem to cover the polymer surface (Fig. 6(ii)). After the third run (Fig. 6(iii)–(iv)) the surface seems more layer-structured and contains less relief than the as prepared catalyst pointing out the erosion of the surface during utilization.

3.4.3. Discussion about initial activation of PVF^f–TiO_2–Fe oxide and increase of synergistic effects

The enhancement of PVF^f–TiO_2–Fe oxide photo-activity after use, presented in Fig. 4, can be assigned to different phenomena occurring on material surface: (i) continuation of the functionalization of the polymer surface and decreasing of Fe/C ratio during first run may favor substance adsorption, iron re-adsorption and polymer substrate stabilization which increase the photocatalyst performances; (ii) leaving of chlorine from PVF^f–TiO_2–Fe oxide surface (Table 2) causes porous tunnel-like structure into the photocatalytic material and induces exchange with other anions (like OH^-, F^-) which might affect positively the catalyst activity; (iii) TiO_2 particles are exposed to the light after the first run due to irreversible iron oxide dissolution. Thus TiO_2 is likely to contribute to the photocatalytic degradation processes.

Besides photo-Fenton oxidation, radical generation and pollutant degradation are induced by photocatalysis occurring both at iron oxide and TiO_2 surfaces (Eqs. (4) and (5)) as well as by synergistic effects of TiO_2 and iron oxide (Eqs. (6)–(8)). More details about these mechanisms were reported in previous works [3,20].

$$\text{Fe oxide} + h\nu \rightarrow \text{Fe oxide}\,(e^- + h^+) \quad (4)$$

$$TiO_2 + h\nu \rightarrow TiO_2\,(e^- + h^+) \quad (5)$$

$$=\text{Fe(III)} + h\nu + TiO_2 \rightarrow =\text{Fe(IV)} + TiO_2\,(e^-) \quad (6)$$

$$\text{Fe oxide} + TiO_2\,(e^-) \rightarrow \text{Fe oxide}\,(e^-) + TiO_2 \quad (7)$$

$$\text{Fe oxide}\,(e^-) + =\text{Fe(III)} \rightarrow \text{Fe oxide} + =\text{Fe(II)} \quad (8)$$

In all the equations, =Fe(II) and =Fe(III) represent iron species in solid or solution phase.

3.5. Effect of reaction conditions on photocatalytic activity

3.5.1. Effect of pH

Even though the system PVF^f–TiO_2–Fe oxide/H_2O_2/light exhibited high photocatalytic activity for the degradation and mineralization of 0.18 mM HQ at natural initial pH, it is relevant to explore its activity at other initial pHs. The experiments were performed at initial pHs 7.1, 5.8, 3.4 and they were not controlled during the experiment. The influence of initial pH on HQ degradation and mineralization by PVF^f–TiO_2–Fe oxide/H_2O_2/light is shown in Fig. 7(i). Total HQ abatement was rapidly observed in the studied initial pH range (traces a–c). Fig. 7(i) shows that the initial (first 30 min) pH value did not affect substantially the degradation rates. The initial degradation (30 min) and mineralization (120 min) rates were increased only 1.5-fold varying initial pH from 7.1 to 3.4.

Fig. 7(ii) illustrates the pH evolution during the process. While at initial pH of 3.5, this value remained nearly constant (trace a), for initial pHs 5.7 and 7.1, the pH decreased during the process to reach a minimum value around 4.5 at 120 min (traces b and c). Then after, pH slightly increased probably due to the mineraliza-

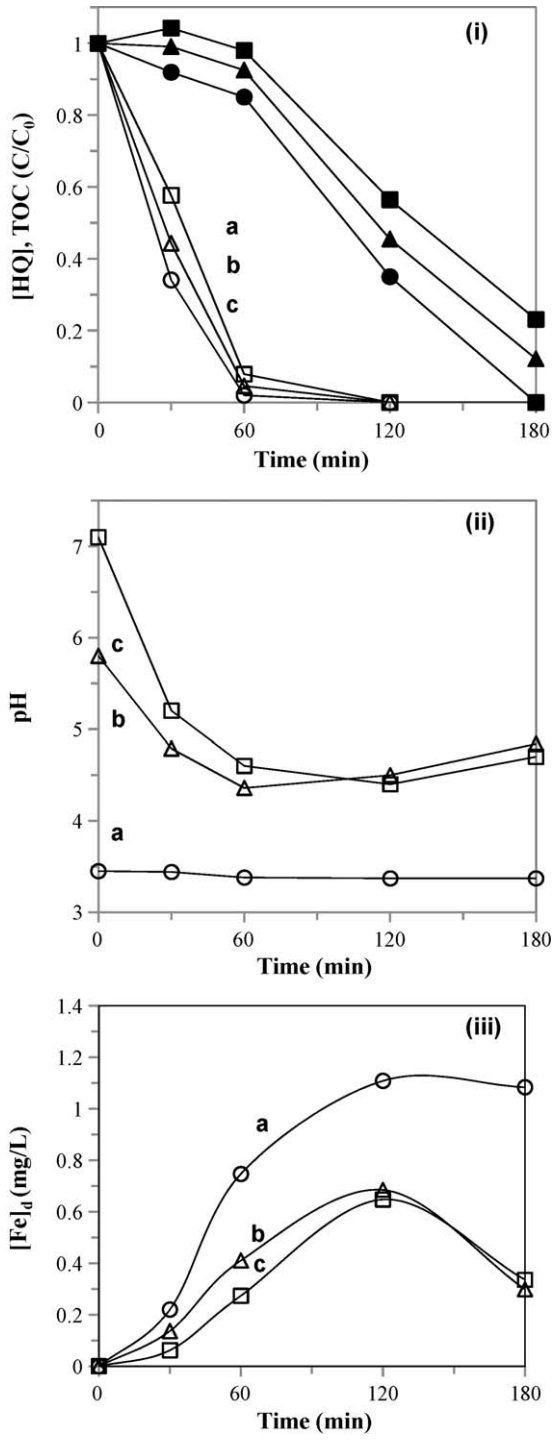

Fig. 7. Variation of (i) HQ and TOC normalized concentrations, (ii) pH and (iii) $[Fe]_d$ during degradation of 0.18 mM of HQ, 1.6 mM H_2O_2, 30 °C, 75 cm^2 of PVF^f–TiO_2–Fe oxide under solar simulation and at different initial pHs. (a) 3.4, (b) 5.8, and (c) 7.1.

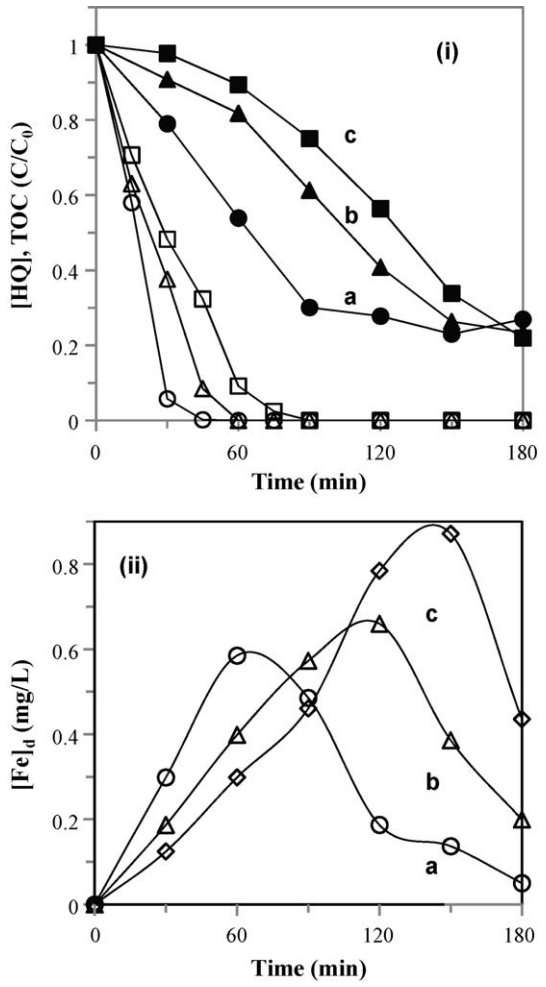

Fig. 8. Variation of (i) HQ and TOC normalized concentrations and (ii) dissolved iron concentration during degradation of 0.18 mM of HQ, 1.6 mM H_2O_2, initial pH 5.7, 75 cm^2 of PVF^f–TiO_2–Fe oxide under solar simulation and at different temperatures: (a) 55 °C, (b) 40 °C, (c) 30 °C.

tion of aliphatic acid intermediates generated during the first step of HQ photocatalytic degradation. Two possible reasons for initial acidification are: (i) carboxylic acid formation due to degradation processes (the final pH values are coherent with their acidity constants) and (ii) photoinduced iron leaching producing H^+ (Eq. (15)).

The $[Fe]_d$ measured during the processes (Fig. 7(iii)) increased as the pH becomes more acidic. A final $[Fe]_d$ of 1.1, 0.3 and 0.3 mg/L for initial pHs of 3.4, 5.8, 7.1, respectively, was measured (Fig. 8) corresponding to an augmentation of 3.5-fold as the pH decreases.

The results shown in Fig. 7 (trace c) suggest that it may exist a pH interval where iron dissolution is minimal and photo-activity is high since 40% of HQ was degraded at $5 < pH < 7$ with less than 0.1 mg/L of dissolved iron. Further experiments using pH regulation are required in order to confirm this hypothesis.

The relative independence of degradation rates from the initial pH can be assigned to several phenomena: (i) for PVF^f–TiO_2–Fe oxide/H_2O_2/light system, semiconductor photocatalysis and synergistic action of TiO_2 and iron oxide participate in observed HQ abatement [3]; (ii) the reaction pH decreased to a value near 5 after 30 min.

3.5.2. Effect of temperature

The results obtained for HQ degradation by the system PVF^f–TiO_2–Fe oxide/H_2O_2/light at three different temperatures (30, 40, 55 °C) are presented in Fig. 8(i). The reaction rates increase when temperature increases due to the exponential dependency of the kinetic constant with the reaction temperature (Arrhenius). The activation energy was calculated using pseudo first order rates (k_1) and plotting $\ln(k_1)$ versus $1/T$. The slope multiplied by the gas constant gives E_a = 57 kJ/mol. Thus the oxidation of HQ needs low activation energy when PVF^f–TiO_2–Fe oxide was used as catalyst. These values suggest ion–molecule and radical–molecule reactions requiring activation energy besides the radical–radical reactions that need no E_a.

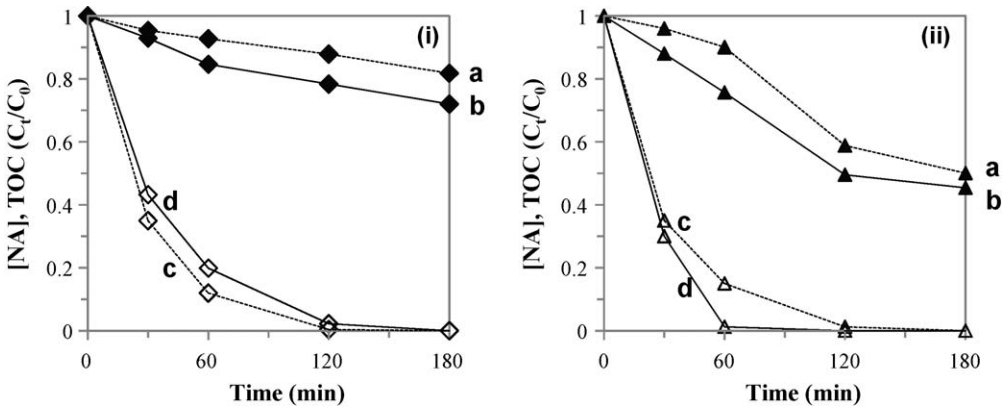

Fig. 9. Variation of HQ and TOC normalized concentrations during degradation of 0.18 mM NA by (i) 75 cm^2 of PVF^f–TiO_2–Fe oxide, (ii) 2 mg/L Fe^{2+}: TOC removal (a) in presence and (b) without NaCl; NA degradation (c) in presence and (d) without NaCl (experimental conditions: initial pH 6.5, 30 °C, 3.2 mM H_2O_2, 0.86 M NaCl under solar simulation).

Fig. 8(i) shows that the TOC removal is a function of the reaction temperatures. After 90 min treatment, 70% TOC is removed at 55 °C (trace a) whereas 40% and 25% TOC was removed at 40 °C (trace b) and 30 °C (trace c), respectively. When the temperature increases (up to 55 °C), the H_2O_2 consumption accelerates and mineralization processes stop sooner than at a lower temperature. Thus for the trace a in Fig. 8(i), the TOC abatement is slowed and stopped by a total H_2O_2 consumption after 90 min treatment.

The degradation and initial mineralization (first 60 min in Fig. 8(i)) rates increased 6- and 5-fold respectively when temperature increased from 30 to 55 °C. This is valuable as solar light can be used to activate this process since it is usually accompanied by a significant increase in the temperature of the bulk reactor. Although one could expect that an increase of temperature might increase extend of leaching, it was not the case with the PVF^f–TiO_2–Fe oxide composite as shown in Fig. 8(ii). Iron leaching initial (first 30 min) rates were accelerated by the temperature of the treatment but the maximal concentration of dissolved iron was inversely proportional to temperature with a $[Fe]_d$ around 0.6, 0.7 and 0.9 mg/L for 55 °C (trace a), 40 °C (trace b) and 30 °C (trace c), respectively.

3.5.3. Effect of NaCl

The effect induced by the addition of NaCl (5 g/L) on NA degradation and mineralization mediated by the systems PVF^f–TiO_2–Fe oxide/H_2O_2/light (i) and Fe^{2+}(2 mg/L)/H_2O_2/light (ii) is illustrated in Fig. 9. The salt adjunction was detrimental for the mineralization process of both homogeneous and heterogeneous systems. The initial mineralization rate (first 60 min) was around 2 times lower in presence (trace a) than in absence (trace b) of salt. For NA degradation in absence of salt, the rate relative to homogeneous system (trace d Fig. 9(ii)) was 3 times higher than those of heterogeneous system (trace d Fig. 9(i)). However, in the presence of salt (trace c), the rates observed were similar for homogeneous and heterogeneous systems.

This comparison suggests that the heterogeneous system is advantageous for the treatment of saline wastewater since the degradation process is slightly faster in salt presence.

It is known that the inhibitory effect of Cl^- on Fenton reaction is due to the scavenging of $OH^\bullet$ by this ion [21]. Thus for PVF^f–TiO_2–Fe oxide/H_2O_2/light system: (i) mineralization process seems largely controlled by photo-Fenton reaction initially induced by $OH^\bullet$ attacks and then by charge transfers occurring on iron oxide surface or dissolved complexes with intermediates; (ii) degradation process is heterogeneous and involves charge transfers from catalyst surface to pollutant rather than the participation of $OH^\bullet$.

3.6. Long-term stability and self-degradation of PVF–Fe oxide and PVF^f–TiO_2–Fe oxide

The long-term stability of PVF–Fe oxide and PVF^f–TiO_2–Fe oxide was studied by two methods: (i) the conventional way which is the evaluation of catalytic performances during repetitive substance degradations; (ii) the self-degradation test which consists in irradiating the photocatalysts in the absence of dissolved organic substance, but in the presence of H_2O_2. This last stability test simulates highly reactive conditions and aims to determine if the substrates as well as overall photocatalytic performance are altered by self-degradation. Fig. 10 depicted repetitive HQ mineralization (eight catalytic cycle and one self-degradation test). Between two runs, the catalysts were thoroughly washed with distilled water. In Fig. 10(i), the PVF–Fe oxide catalytic activity remains constant during five recycling (traces b–f) with about 65% TOC removal after 3 h treatment. For this catalyst, the initial TOC increase due to polymer degradation still occurs until the fifth run. The self-degradation test (after 18 h) induced an important and irreversible loss of 50% of photocatalytic activity (traces g–h). In contrast, for the PVF^f–TiO_2–Fe oxide (Fig. 10(ii)), the self-degradation test (after 6 h) induces only a 10% loss of catalytic activity between runs 2 and 3. The photo-activity recovery was reached during the next runs (traces d–f), and finally decreases

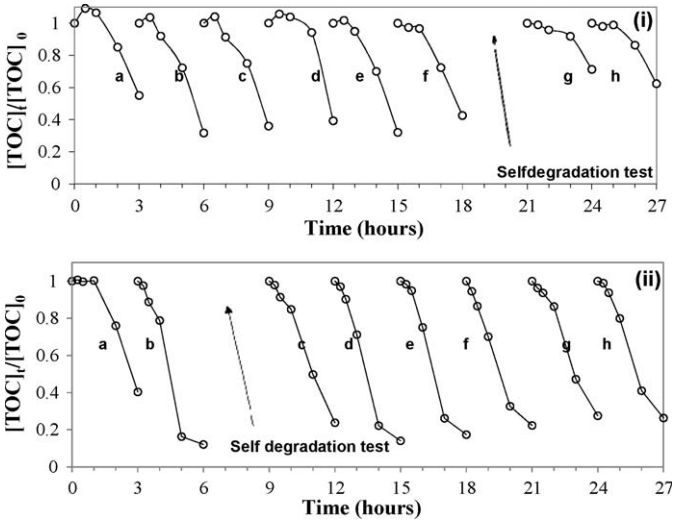

Fig. 10. TOC removal during repetitive HQ photocatalytic degradation by (i) PVF–Fe oxide and (ii) PVF^f–TiO_2–Fe oxide (experimental conditions: 0.18 mM HQ, 30 °C, solar simulation, initial pH 5.7, H_2O_2 1.6 mM).

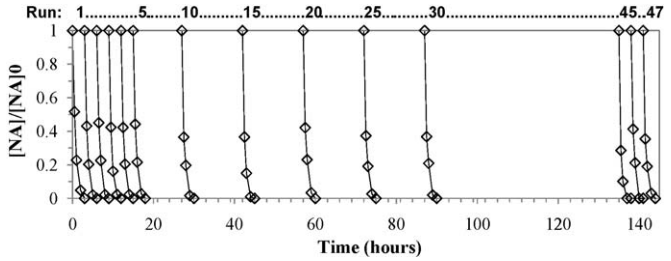

Fig. 11. Repetitive NA degradation (experimental conditions: 0.18 mM NA, 30 °C, solar simulation, initial pH 6.5, PVF^f–TiO_2–Fe oxide 75 cm^2, H_2O_2 3.2 mM).

slowly (traces f–h). At the end of the self-degradation test, dissolved iron concentration was measured and reaches a value above 1 mg/L. From these results, the two tested catalysts are stable toward repetitive HQ photocatalytic degradations whereas only the PVF^f–TiO_2–Fe oxide is stable toward self-degradation.

Fig. 11 represents a stability test repeating NA photocatalytic degradation mediated by PVF^f–TiO_2–Fe oxide, recording NA evolution as a function of time. These results show that the PVF^f–TiO_2–Fe oxide is extremely stable during 47 consecutive runs corresponding to about 150 h of operation. The degradation rate relative to the first run, an average of runs 2–6, 10–30 and 45–47 was calculated. Surprisingly, instead of a slow decrease of the degradation rates, a slow increase was observed. The rate undergoes a 1.5-fold increase between runs 2–6 and runs 45–47. These results suggest that the presence of TiO_2 particles deposited on PVF substrate not only increased iron oxide formation and deposition on polymer surface [3] but also other beneficial effects: (i) as long as the PVF^f–TiO_2–Fe oxide is used, the TiO_2 uncovering and exposition to light, induced by iron photo-dissolution, increases the Ti/Fe surface concentration (Table 2) which increases the synergistic effects and the degradation rates and (ii) the catalyst was protected from self-degradation since TiO_2 diminished the contact between radicals and polymer surface and can trap charges which otherwise would degrade the polymeric substrate.

3.7. Reversible iron dissolution

Iron leaching from oxides to solution is well documented and is believed to occur via photo-reductive dissolution. The leaching process can be described as follows (Eqs. (9)–(14)): (i) carboxylate ligands (like aliphatic acids (AA) produced by organic pollutant degradation (Eq. (9)) can form surface Fe(III)–carboxylate complexes (Eq. (10)); (ii) The formed surface or dissolved complexes are thought to participate in ligand to metal charge transfer reactions (Eq. (11)). For dissolution to take place, the Fe(II) sites formed at the surface of the Fe(III) oxide must detach (Eq. (12)). In the presence of oxidant, the surface Fe(II) sites may be re-oxidized before it can detach (Eq. (13)) [12,14]

$$HQ + PVF^f\text{–}TiO_2\text{–Fe oxide} + H_2O_2 + h\nu \rightarrow \rightarrow \rightarrow AA \quad (9)$$

$$=Fe(III)OH + HC_2O_4^- \leftrightarrows =Fe(III)C_2O_4 + H_2O \quad (10)$$

$$=Fe(III)C_2O_4 + h\nu \leftrightarrows =Fe(III)C_2O_4{}^* \rightarrow =Fe(II) + CO_2 + CO_2{}^- \quad (11)$$

$$=Fe(II) \rightarrow Fe^{2+} + = \quad (12)$$

$$=Fe(II) + Ox \rightarrow =Fe(III) + Red \quad (13)$$

Recently Sherman [19] reports that leaching of iron species from the iron (hydr)oxide surface to the aqueous solution is also possible via photo-reduction of bounded aqua-complexes (Eqs. (14) and (15)).

$$=Fe(III)(H_2O) + h\nu \leftrightarrows =Fe(II)(H_2O)^+ \quad (14)$$

$$2=Fe(II)(H_2O)^+ \rightarrow 2Fe^{2+} + H_2O_2 + 2H^+ \quad (15)$$

During this work, leaching of iron species from oxide surface to the solution was probably caused by the simultaneous presence of light, dissolved organic substances (or polymer substrate) and H_2O_2.

The pH of the reaction media influenced considerably the iron photo-dissolution process since the more the initial pH is acidic the more iron dissolved was found in solution (see Section 3.4.1, in Fig. 7(iii)).

Finally the dissolved iron re-deposition (Eq. (16)) can be explained as follows. First the dissolved Fe(II) species undergo oxidation processes like Fenton reaction producing Fe(III) species. These species are not stable in aqueous phase under the experimental conditions (pH 4.5; absence of dissolved organic ligands) at the end of the treatment. Thus Fe(III) species re-deposit on vacant site (=) located at iron oxide, TiO_2, polymer and reactor surfaces.

$$Fe^{3+} + = \rightarrow =Fe(III) \quad (16)$$

The observed phenomena of dissolved iron concentration depletion could have important theoretical and practical implications and may allow new alternatives for dissolved iron removal in homogeneous photo-Fenton processes.

4. Conclusions

The aimed characteristics for supported TiO_2–Fe oxide as heterogeneous photocatalysts have been reached when using PVF^f–TiO_2–Fe oxide/H_2O_2/light system:

- The photo-dissolution of iron ions and their relative homogeneous contribution to HQ and NA initial mineralization was low.
- HQ and NA photo-assisted degradation rates were high and mostly independent of initial pH and NaCl presence but increased with temperature.
- The film substrate was resistant to self-degradation by generated radicals.
- The photocatalytic activity was highly stable toward repetitive pollutant degradation and it was even slightly increasing after 150 h operation.
- The preparation method proposed is sustainable as it used solar light, water as solvent and low temperatures.

The presence of TiO_2 particles on photocatalyst surface was found to engender three principal beneficial effects: (1) the iron oxide deposition was higher on TiO_2 coated PVF surfaces than in commercial PVF; (2) the initial and long-term activations were assigned to the uncovering of TiO_2 due to irreversible iron dissolution which increased its exposition to light and consequently its synergistic contribution to the overall photocatalytic degradation process; (3) the resistance to self-degradation was assigned to TiO_2 which may act as charge trap and diminish the contact between active iron species and polymer surface.

Acknowledgements

F. Mazille wishes to express his gratitude to Pierre-Yves Pfirter, Nicolas Xanthopoulos and Adrien Rollux for SEM, XPS, and NA degradation, respectively, to Dorothea Spuhler for her precious

help in experiments and in reviewing of phrasing and to John Kiwi and Thomas Schoettl. The authors wish to thank the European Commission for its financial support under the INNOWATECH project (contract No. 036882) within the thematic priority Global Change and Ecosystems of the Sixth Framework Program (FP6-2005-Global 4 – SUSTDEV-2005-3.II.3.2).

References

[1] E. Celik, A.Y. Yildiz, N.F. Ak Azem, M. Tanoglu, M. Toparli, O.F. Emrullahoglu, I. Ozdemir, Mater. Sci. Eng. B 129 (2006) 193–199.
[2] X. Zhang, L. Lei, Appl. Surf. Sci. 254 (2008) 2406–2412.
[3] F. Mazille, T. Schoettl, C. Pulgarin, Appl. Catal. B 89 (2009) 635–644.
[4] A. Moncayo, R.A. Torres-Palma, J. Kiwi, N. Benítez, C. Pulgarin, Appl. Catal. B 84 (2008) 577–583.
[5] J. Bandara, U. Klehm, J. Kiwi, Appl. Catal. B 76 (2007) 73–81.
[6] J.H. Ramirez, C.A. Costa, L.M. Madeira, G. Mata, M.A. Vicente, M.L. Rojas-Cervantes, A.J. Lopez-Peinado, R.M. Martin-Aranda, Appl. Catal. B 71 (2007) 44–56.
[7] W. Song, M. Cheng, J. Ma, W. Ma, C. Chen, J. Zhao, Environ. Sci. Technol. 40 (2006) 4782–4787.
[8] D. Gumy, P. Fernandez-Ibanez, S. Malato, C. Pulgarin, O. Enea, J. Kiwi, Catal. Today 101 (2005) 375–382.
[9] T. Yuranova, O. Enea, E. Mielczarski, J. Mielczarski, P. Albers, J. Kiwi, Appl. Catal. B 49 (2004) 39–50.
[10] Y. Zhiyong, E. Mielczarski, J. Mielczarski, D. Laub, Ph. Buffat, U. Klehm, P. Albers, K. Lee, A. Kulik, L. Kiwi-Minsker, A. Renken, J. Kiwi, Water Res. 41 (2007) 862–874.
[11] Z. Yaping, H. Jiangyong, Appl. Catal. B 79 (2008) 250–258.
[12] B. Sulzberger, H. Laubscher, Mar. Chem. 50 (1995) 103–115.
[13] W.P. Kwan, B.M. Voelker, Environ. Sci. Technol. 36 (2002) 1467–1476.
[14] B.M. Voelker, F.M. Morel, B. Sulzberger Environ. Sci. Technol. 31 (1997) 1004–1011.
[15] E. Viollier, P.W. Inglett, K. Hunter, A.N. Roychoudhury, P. Van Cappellen, Appl. Geochem. 15 (2000) 785–790.
[16] A. Bozzi, T. Yuranova, J. Mielczarski, A. Lopez, J. Kiwi, Chem. Commun. 19 (2002) 2202–2203.
[17] J. Feng, X. Hu, L.Y. Po, Environ. Sci. Technol. 38 (2004) 5773–5778.
[18] J. Cai, J. Liu, Z. Gao, A. Navrotsky, S.L. Suib, Chem. Mater. 13 (2001) 4595–4602.
[19] D.M. Sherman, Geochim. Cosmochim. Acta 69 (2005) 3249–3255.
[20] N. Murakami, T. Chiyoya, T. Tsubota, T. Ohno, Appl. Catal. A 348 (2008) 148–152.
[21] J.J. Pignatello, E. Oliveros, A. MacKay, Crit. Rev. Environ. Sci. Technol. 36 (2006) 1–84.